NANO LETTERS

Letter

pubs.acs.org/NanoLett

Biodegradable Elastomers and Silicon Nanomembranes/Nanoribbons for Stretchable, Transient Electronics, and Biosensors

Suk-Won Hwang,[†] Chi Hwan Lee,[‡] Huanyu Cheng,[§] Jae-Woong Jeong,[∥] Seung-Kyun Kang,[‡] Jae-Hwan Kim,[‡] Jiho Shin,[⊥] Jian Yang,[#] Zhuangjian Liu,[▽] Guillermo A. Ameer,[#] Yonggang Huang,[§] and John A. Rogers*[,‡,○,◆]

[†]KU-KIST Graduate School of Converging Science and Technology, Korea University, Seoul 136-701, Korea

[‡]Department of Materials Science and Engineering, Frederick Seitz Materials Research Laboratory, University of Illinois at Urbana−Champaign, Urbana, Illinois 61801, United States

[§]Department of Mechanical Engineering, Civil and Environmental Engineering, Center for Engineering and Health, and Skin Disease Research Center, Northwestern University, Evanston, Illinois 60208, United States

[∥]Department of Electrical, Computer, and Energy Engineering, University of Colorado, Boulder, Colorado 80309, United States

[⊥]Department of Chemical and Biomolecular Engineering, University of Illinois at Urbana−Champaign, Urbana, Illinois 61801, United States

[#]Department of Biomedical Engineering, Northwestern University, Evanston, Illinois 60208, United States

[▽]Institute of High Performance Computing, 1 Fusionopolis Way, #16-16 Connexis, Singapore 138632, Singapore

[○]Beckman Institute for Advanced Science and Technology, University of Illinois at Urbana−Champaign, Urbana, Illinois 61801, United States

[◆]Department of Chemistry, Mechanical Science and Engineering, Electrical and Computer Engineering, University of Illinois at Urbana−Champaign, Urbana, Illinois 61801, United States

Supporting Information

ABSTRACT: Transient electronics represents an emerging class of technology that exploits materials and/or device constructs that are capable of physically disappearing or disintegrating in a controlled manner at programmed rates or times. Inorganic semiconductor nanomaterials such as silicon nanomembranes/nanoribbons provide attractive choices for active elements in transistors, diodes and other essential components of overall systems that dissolve completely by hydrolysis in biofluids or groundwater. We describe here materials, mechanics, and design layouts to achieve this type of technology in stretchable configurations with biodegradable elastomers for substrate/encapsulation layers. Experimental and theoretical results illuminate the mechanical properties under large strain deformation. Circuit characterization of complementary metal-oxide-semiconductor inverters and individual transistors under various levels of applied loads validates the design strategies. Examples of biosensors demonstrate possibilities for stretchable, transient devices in biomedical applications.

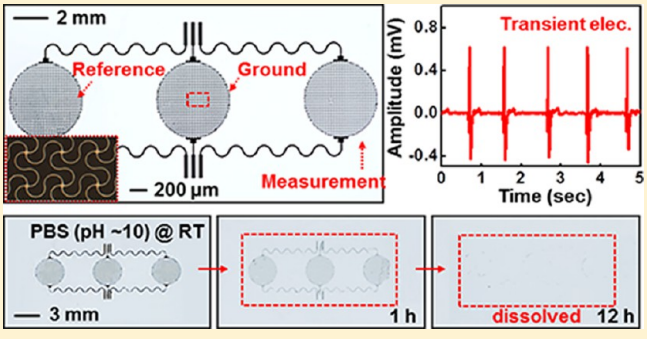

KEYWORDS: *Stretchable, flexible, transient, biodegradable electronics, biosensors*

Advances in inorganic nanomaterials and unconventional fabrication techniques have recently yielded capabilities for broad classes of semiconductor devices and integrated systems that are entirely soluble in biofluids with nontoxic end products.[1−17] Of particular interest are approaches that use single crystalline nanomembranes of silicon (Si NMs)[8−10,14−16] or thin films of zinc oxide[11] as the semiconductor to achieve not only the essential electronic components needed for integrated circuits but also other devices such as solar cells,[8] temperature/strain/hydration sensors,[8,15] multiplexed arrays of photodetectors,[8] mechanical energy harvesters,[11] and radio frequency power scavengers.[9] For Si NMs, the rates of hydrolysis vary between tenths and tens of nanometers per day in groundwater, biofluids and other solutions of interest, where the specific rates depend on temperature, pH, ionic concentration, doping level of the silicon, and other factors.[8,14,16] These and related electronic systems combine such semiconductors with Mg or other dissolvable metals (e.g., Zn, Fe, W, Mo) for interconnects and electrodes;[18] MgO and

Received: October 17, 2014
Revised: February 8, 2015
Published: February 23, 2015

DOI: 10.1021/nl503997m
Nano Lett. 2015, 15, 2801−2808

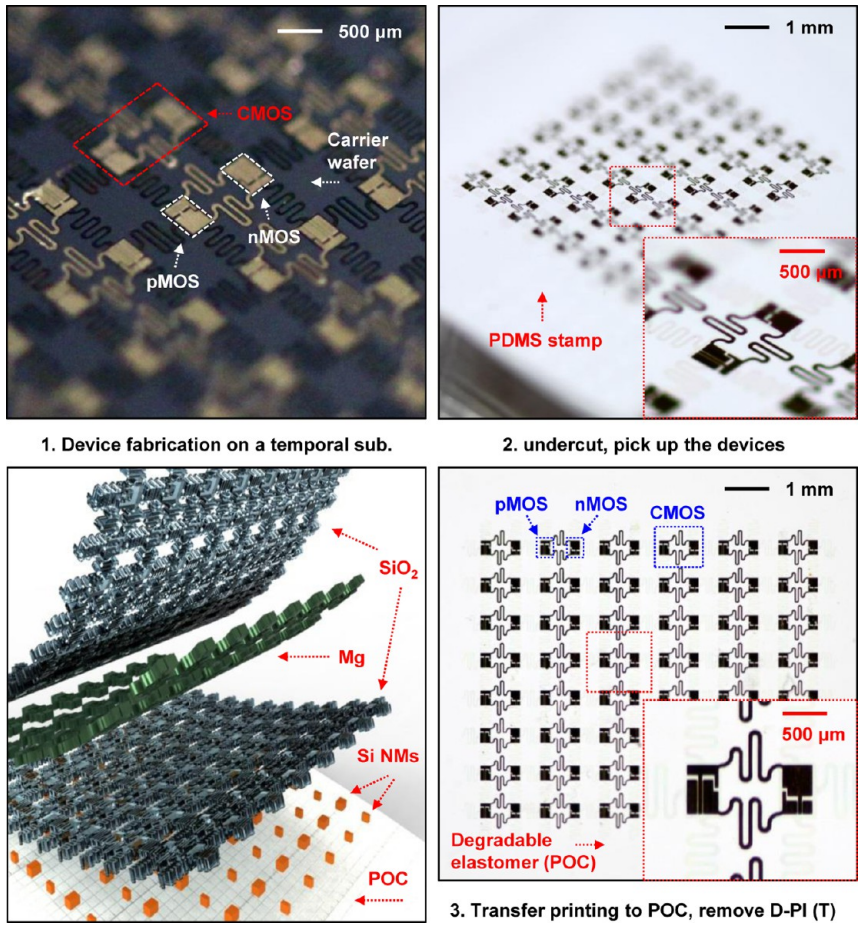

Figure 1. Images and illustrations of stretchable arrays of transient silicon CMOS devices on biodegradable elastomer substrates. These systems incorporate CMOS inverters on POC substrates. Transient CMOS inverters fabricated on a silicon wafer in a stretchable configuration (top left) after release and retrieval onto a slab of PDMS and removal of underlying layer of D-PI layer (top right) and after transfer printing onto a biodegradable elastomer and removal of top D-PI layer to complete the device (bottom right). Schematic exploded view illustration (bottom left) of the various layers, that is, Mg for electrodes/interconnects, silicon dioxide (SiO_2) for gate/interlayer dielectrics, Si NMs for semiconducting elements and POC for substrate/encapsulating materials.

SiO_2 or SiN_x for dielectrics/encapsulating layers;[8,19] biodegradable polymers (e.g., silk, poly lactic-*co*-glycolic acid (PLGA), polycaprolactone (PCL), polylactic acid (PLA)),[8,15] or metal foils for substrates/packaging materials. In addition to their possibility for use in temporary biomedical implants, this type of physically "transient" device technology has potential applications in degradable environmental monitors/sensors, disposable consumer gadgets, "unrecoverable" electronics, and hardware-secure digital memories. Past work demonstrates capabilities for forming devices in rigid or flexible formats.[4,8−11,15] In many cases, particularly those that require integration with the human body, mechanical stretchability (i.e., ability to accommodate strains ≫1%) provides critically important advantages.[20,21] Here we describe transient electronic devices and sensors that use Si NMs and nanoribbons (NRs) in optimized configurations on a biodegradable elastomer (poly(1,8-octanediol-*co*-citrate), POC) to yield systems that can be reversibly stretched to strains of up to ∼30% with linear elastic mechanical responses. The electrical characteristics of the resulting devices are similar to those that use nontransient construction and rigid, planar substrates. Experimental and theoretical studies illustrate the underlying behaviors of the materials and their responses to mechanical deformation. Sensors of pH and skin-mounted monitors of electrophysiology (EP) provide two application examples.

Figure 1 presents optical micrographs and an exploded view schematic illustration of an array of stretchable, transient complementary metal-oxide-semiconductor (CMOS) inverters. Device fabrication begins with a series of doping processes on silicon on insulator (SOI, SOITEC, France) wafers, to create lightly doped p-well (p^-) and heavily doped regions (p^+, n^+) for contacts of both p- and n-channel metal-oxide-semiconductor field-effect transistors (MOSFETs). Removal of the buried oxide with hydrofluoric acid (HF) releases the doped silicon device layer to yield isolated Si NMs. Transfer printing delivers these Si NMs onto a silicon wafer coated with a bilayer of poly(methyl methacrylate) (PMMA, Sigma-Aldrich, U.S.A.) and diluted polyimide (D-PI). Reactive ion etching (RIE, Plasmatherm) of the Si NMs with sulfur hexafluoride (SF_6) defines the active areas of the devices. Plasma-enhanced chemical vapor deposition (PECVD) of silicon dioxide (SiO_2) yields the gate and interlayer dielectrics. A patterned thin film of Mg formed by electron beam evaporation serves as source, drain, and gate electrodes as well as interconnects. A uniform overcoat of PECVD SiO_2 encapsulates the entire system (Figure 1, top left). Removing the PMMA by immersion in acetone enables release onto the surface of a

DOI: 10.1021/nl503997m
Nano Lett. 2015, 15, 2801−2808

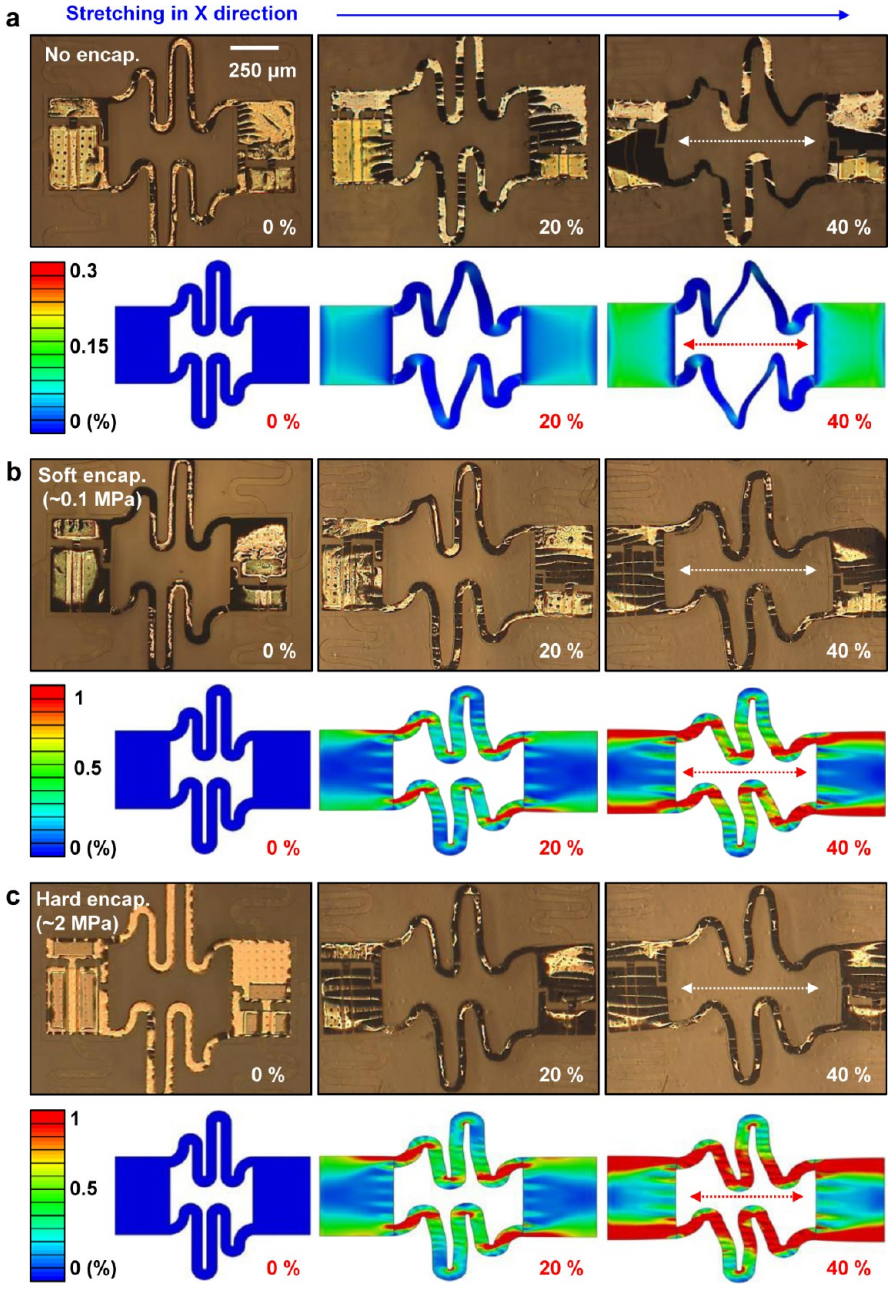

Figure 2. Experimentally observed and calculated distributions of strain in stretchable, biodegradable CMOS inverters. Optical microscope images of CMOS inverters that consist of transistors joined by deformable interconnects for stretching up to ~40% (top) and corresponding results from Finite Element Analysis (FEA, bottom). Cases for (a) no encapsulation, (b) soft encapsulation (0.1 MPa), and (c) hard encapsulation (2 MPa).

slab of polydimethylsiloxane (PDMS) (Figure 1, top right), for transfer onto a biodegradable elastomer substrate, POC (Figure 1, bottom right). Polydiolcitrates represent a unique and interesting platform of elastomeric polyesters that exhibit versatility regarding fundamental and functional design strategies that can be used to meet the goals of a wide range of applications. Similar fabrication procedures are used for all of the various devices reported here. Details appear in Methods.

As explored in previous reports on nontransient stretchable Si NM electronics,[22,23] layouts that include device islands connected by serpentine and/or noncoplanar interconnects allow the system to accommodate large deformations without fracture. Here, the interconnects undergo in- and out-of-plane buckling in response to tensile loads, whereas the islands remain flat and undeformed. The buckling process induces bending strains that are typically orders of magnitude smaller than the applied tensile strains. Additionally, the interconnects often involve metal encapsulated above and below by thin polymer layers, thereby placing the metal near the neutral mechanical plane, to minimize bending strains. We expect the fatigue properties under cyclic loads to be similar to those of related, but nontransient, stretchable systems. These same strategies prove valuable in the context of transient, stretchable Si NM systems introduced here. The results shown in Figure 1a illustrate arrays of stretchable, transient CMOS inverters with three different types of interconnects. Finite element analysis (FEA) reveals the mechanics associated with each case; a representative example appears in Figure 2a (see Supporting Information Figures S1−S3 and movies S1−S2 for additional information). For device islands that are bonded to the

DOI: 10.1021/nl503997m
Nano Lett. 2015, 15, 2801−2808

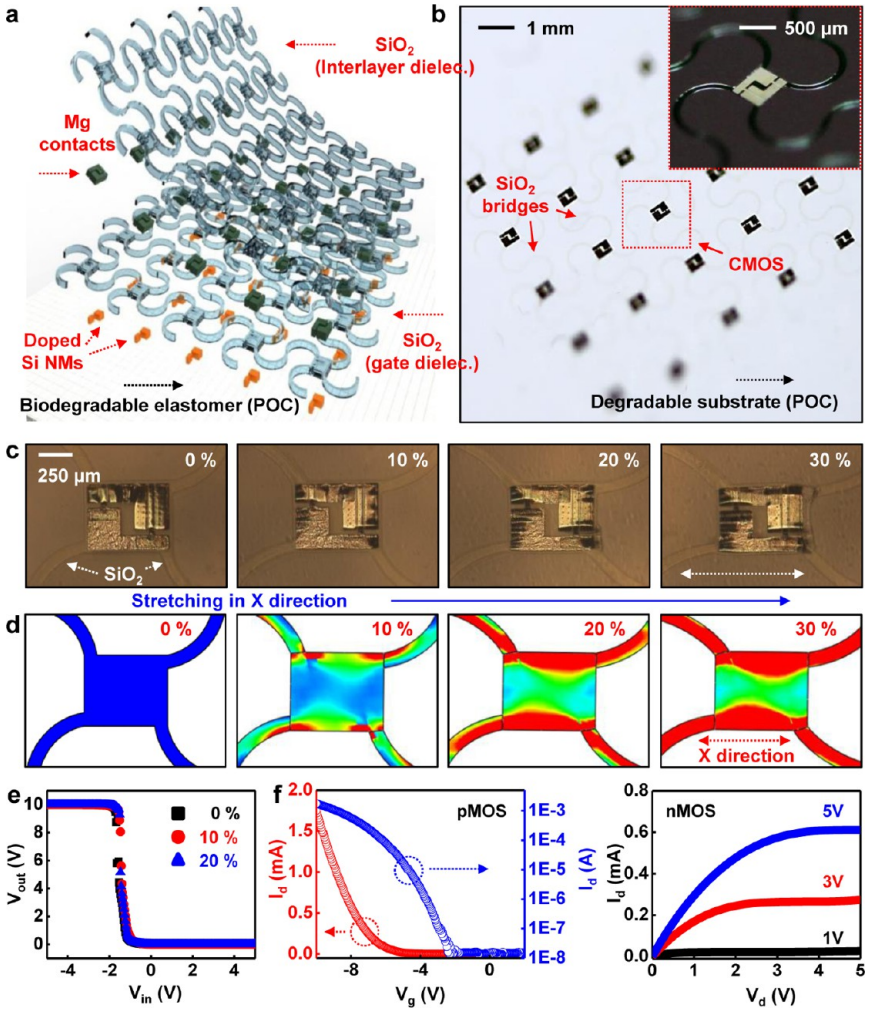

Figure 3. Evaluation of the distributions of strain in CMOS inverters interconnected in a filamentary serpentine (FS) mesh. (a) Schematic exploded view illustration of the device. (b) Image of an array of CMOS inverters with a magnified view in the inset. (c) A set of micrographs before and after applying external strains up to 30% in the *x*-direction. (d) Computed results for principal strain in regions of the FS structure that correspond to micrographs in (c). (e) Electrical characteristics of a representative CMOS inverter at a strain up to 20%. (f) Linear and log-scale transfer curves of a typical p-MOSFET (left) and current−voltage characteristics of a typical n-type MOSFET (right) with different gate biases.

substrate and interconnects that are not, the elastic deformation is predicted to be >40%, determined from the distribution of strain in the Mg (bottom panels of Figure 2a). A top layer encapsulation of POC can enhance the bonding and protect the devices from the environment. The top panels in Figure 2b,c show optical images collected from experiments, where partially cured (Figure 2b, Young's modulus of 0.1 MPa) and fully cured (Figure 2c, Young's modulus of 2 MPa) layers of POC provide encapsulation. FEA shows that the interfacial stresses decrease as the Young's modulus of encapsulation material increases, consistent with the role of this layer in preventing delamination. As shown in the bottom panels of Figure 2b,c, the maximum principal strain increases dramatically when freestanding interconnects are replaced by fully bonded ones. The maximum principal strain in the interconnects increases slightly from soft encapsulation to hard encapsulation. An ultrasoft encapsulation (Supporting Information Figure S2b, Young's modulus of 0.1 KPa) leads to strains that differ by only <3% from the soft encapsulation case. This result highlights the value of substrate chemistries that allow strong, selective bonding only at the islands, as is well established for the case of a nontransient elastomer like silicone. Modifications to POC for this purpose represent topics of current work.

An alternative architecture for stretchable electronics, first introduced in devices with mechanical properties matched to the epidermis (i.e., epidermal electronic systems),[20] exploits a mesh design constructed of filamentary serpentine (FS) traces. Figure 3a,b presents an exploded view schematic illustration and optical images of transient CMOS inverters using this type of layout. Here, FS bridges of SiO_2 connect small, isolated device islands. The images and maximum principal strain distributions (in percent) in Figure 3c,d correspond to an array of CMOS inverters formed in this manner; the stretchability reaches ∼30% in the *x*-direction (more results on FEA appear in Supporting Information Figure S4 and Movie S3). Portions of the device structures begin to delaminate after stretching to more than 30%. As for the examples of Figure 2, the stretchability can be enhanced through the use of nonbonded interconnects. Corresponding electrical characteristics of a representative CMOS inverter appear in Figure 3e. The output voltages remain constant during applied strain (black, 0%; red, 10%; blue, 20%) with gain and threshold voltage (V_{th}) of ∼60 and −1 V, respectively, at a supply voltage of 10 V (V_{dd})

DOI: 10.1021/nl503997m
Nano Lett. 2015, 15, 2801−2808

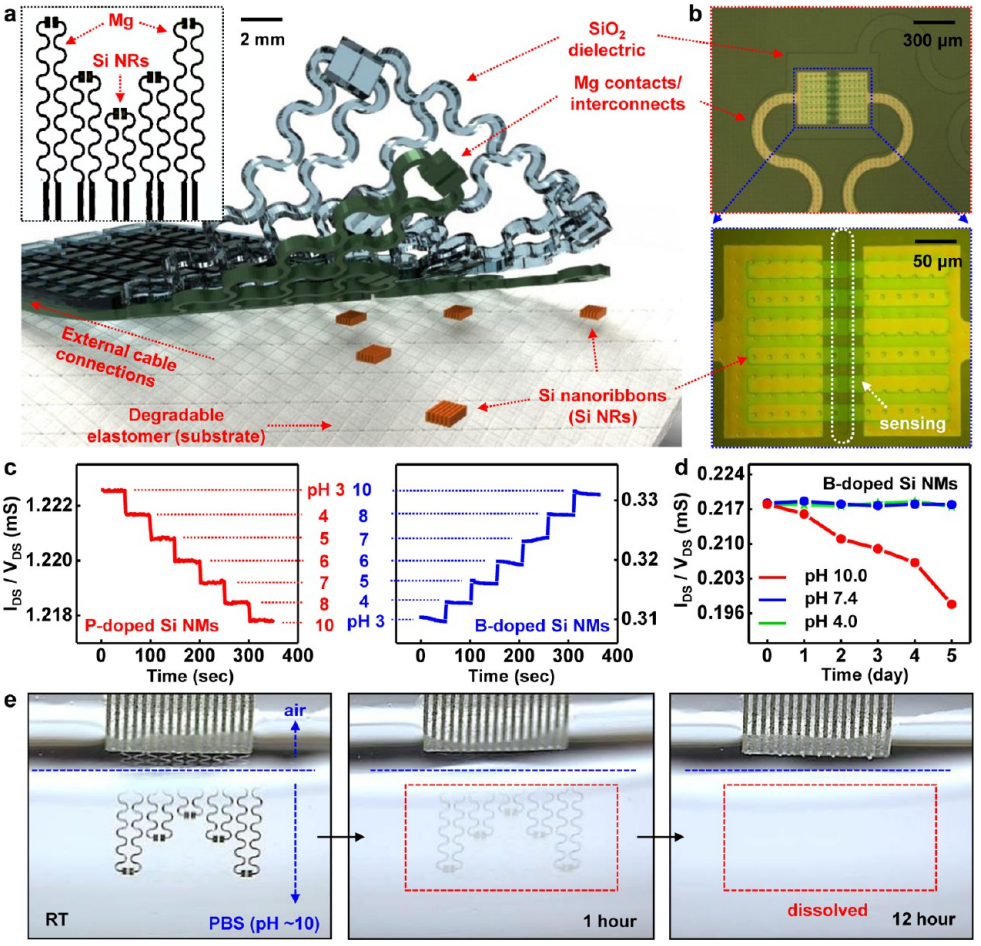

Figure 4. Biodegradable, stretchable pH sensors based on doped Si NRs. (a) Exploded view schematic illustration of a device with a photograph in the inset. (b) Optical microscope image of an individual pH sensor (top) and its magnified view. (c) Measurements of the conductance of devices submerged in solutions with various pH (from 3 to 10) for the cases of phosphorus (left) and boron (right) doped Si NRs. (d) Changes in conductance of heavily boron-doped Si NRs (~200 nm thick) while submerged in phosphate buffer solution (PBS, 0.1 M, pH 4–10, Sigma-Aldrich, U.S.A.) at 37 °C. (e) Images at various stages of dissolution of a device during immersion in PBS (pH 10) at room temperature.

(Supporting Information Figure S5). The negative threshold voltage of the inverters arises from the high negative threshold voltage of the p-type MOSFETs. Figure 3f presents transfer curves in linear (red) and logarithmic (blue) scales for a typical p-channel MOSFET (left) and current–voltage characteristics for a typical n-channel MOSFET (right). The mobilities are ~70 $cm^2/V{\cdot}s$ (p-type) and ~400 $cm^2/V{\cdot}s$ (n-type); the on/off (I_{on}/I_{off}) ratios are ~10^5.

This type of stretchable mechanics is important for applications such as those in biomedicine, where conformal lamination onto the time-dynamic, curvilinear surfaces of the skin or other organs of the body is critically important. As an example of a type of transient biosensor with utility in this area, Figure 4a presents a schematic illustration of stretchable pH monitors built using doped Si NRs (length, width, and thickness: 500 μm, 40 μm, and 300 nm, respectively) functionalized with 3-aminopropyltriethoxysilane (APTES). Mg serves as the electrodes and interconnects, SiO_2 serves as the interlayer dielectrics and encapsulants, and POC serves as the substrate. The inset shows an image of the device. Figure 4b provides an optical micrograph of an individual pH monitor (top) and a magnified view (bottom). Figure 4c shows measured changes in conductance of devices constructed with phosphorus (left) and boron (right) doped Si NRs (~$10^{20}/cm^3$ for both cases), as a function of time when exposed to solutions with different pH. Here, the $-NH_2$ and $-SiOH$ groups[24] on the functionalized surfaces of the Si NRs undergo protonation to $-NH_3^+$ at low pH and deprotonation to $-SiO^-$ at high pH. Resulting changes in the surface charge electrostatically gate the transport in the silicon by depleting or accumulating charge carriers. The result is that the conductance of phosphorus and boron-doped Si NRs descends and ascends, respectively, in a series of distinct steps with pH (from 3 to 10) in aqueous solutions.[25,26] The sensitivities of representative devices are 0.1 ± 0.01 and 0.3 ± 0.02 μS/pH for phosphorus and boron doped Si NRs, respectively. The latter results are in a range of those observed in boron-doped silicon nanowires (Si NWs) constructed in the usual way on silicon wafer substrates (0.1–4 μS/pH).[25,27,28] This sensitivity depends on doping concentration, fabrication method (bottom-up, top-down), and geometry (surface-to-volume ratio) of the Si NWs, as well as local gate controls.[27,28] To establish the time frame of viable measurements of pH with these transient devices Figure 4d shows changes in conductance of highly boron-doped Si NRs (similar doping level used in Figure 4c) evaluated in test structures during immersion in phosphate buffer solutions (PBS, 0.1 M, Sigma-Aldrich, U.S.A.) with different pH (from 4 to 10) for 5 days at 37 °C. In PBS with pH 7.4 at 37 °C (0.1

DOI: 10.1021/nl503997m
Nano Lett. 2015, 15, 2801–2808

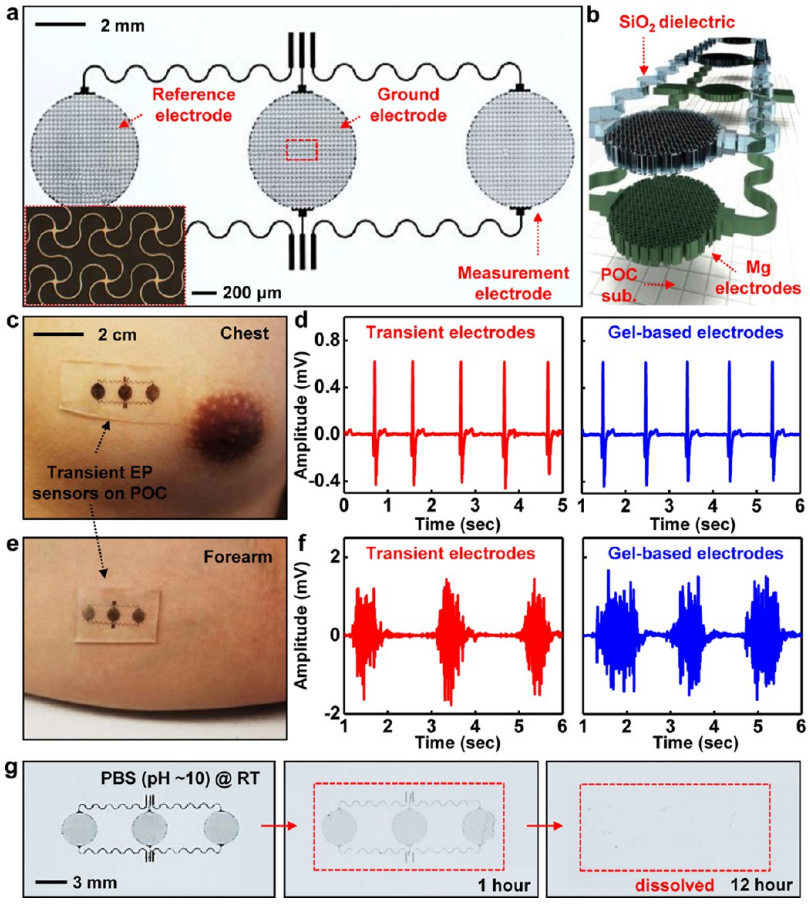

Figure 5. Capacitive biodegradable, stretchable EP sensors. (a) Optical image of a device and magnified view of the FS mesh electrode structure (inset). (b) Exploded view schematic illustration. (c) Photograph of a device mounted on the chest for measurement of ECG (left). ECG collected using a biodegradable (middle) and standard gel-based (right) device. (d) Photograph of the EP sensor located on the forearm for measurement of EMG (left). EMG collected using a biodegradable (middle) and standard gel-based (right) device, while clenching the first every 2 s. (e) A series of images of dissolution of a device in PBS (pH 10) at room temperature.

M), the conductance of the Si NRs (heavily boron-doped) changes by ~1% or less during immersion for 5 days. This dissolution behavior is consistent with thickness changes reported previously for highly boron-doped Si NMs in similar solutions.[16] The dissolution rates depend on the types and concentrations of ions in solution. For example, the rate in PBS (pH 7.4, 0.1 M) is ~20 times slower than in PBS (pH 7.4, 1 M) and ~1.5 times faster than that in PBS (pH 7.4, 0.05 M).[14] (Even for fixed concentration, the type of ions in the PBS can have strong effects. Recent changes in formulation of a commercial PBS (Sigma-Aldrich, U.S.A.) increased the dissolution rate by ~20 times, the details of which will be described elsewhere.) The most relevant rates, of course, are those that occur in biofluids of interest. Dissolution studies of highly doped Si (boron and phosphorus) in bovine serum at 37 °C appear in Supporting Information Figure S6. In both cases, the dissolution rates are ~2.5 nm/day, which is somewhat slower than calculated values from previous reports[14,16] likely due to differences in doping levels. Unencapsulated pH monitors have potential for use over limited periods of time at low or near neutral pH because the measured conductance (in the case of bovine serum) exhibits negligible changes (less than 1%) after a day in such conditions. At higher pH (pH 10), a linear decrease in conductance (less than 10%) during this period occurs, as expected. The time durations for stable operation can be extended by including overcoats of ultrathin dielectric insulators that exhibit slow dissolution rates, such as SiO_2 or SiN_x.[19] Although this type of encapsulation can affect the response, previous studies suggest that ultrathin coatings of SiO_2 with surface treatments can enable useful levels of sensitivity.[29,30] Figure 4e presents a set of images at various stages of dissolution of a pH sensor while immersed in PBS (pH 10, Sigma-Aldrich, U.S.A.) at room temperature. The Mg electrodes completely disappear after 12 h via reactive dissolution (i.e., hydrolysis), and other components (Si, SiO_2, POC) dissolve slowly in several weeks with rates similar to those reported in previous articles,[8,14,16,19,31] in which the kinetics depend strongly on temperature, and pH and ionic content/concentration of solutions, as well as the morphologies of the materials. The rate of dissolution of POC can be controlled/tuned by adjusting the cross-linking density or using different monomers.[31]

As another application example, Figure 5a,b presents optical images and schematic illustrations of a stretchable, transient EP sensor. The device includes thin layers of Mg (300 nm) and SiO_2 (100 nm) in the form of FS meshes (Figure 5a, inset) for measurement, ground and reference electrodes, and connecting leads. The Mg electrodes couple to the skin through a thin sheet of POC in a sensing mechanism that relies on displacement currents generated by capacitive coupling through the SiO_2. This arrangement enables EP measurements with levels of fidelity that are comparable to those of conventional

DOI: 10.1021/nl503997m
Nano Lett. 2015, 15, 2801−2808

gel electrodes.[32] High quality of electrocardiograms (ECG) and electromyograms (EMG) can be recorded by attaching transient, capacitive EP sensors on the chest (Figure 5c) and the right forearm (Figure 5e) of a volunteer (age 27). The resulting ECG (Figure 5d) and EMG (Figure 5f) data (red) compare quantitatively to those collected with conventional gel-based electrodes (blue). Figure 5g shows a set of images of a EP sensor during dissolution when submerged in PBS (pH 10) at room temperature. The transient electronic materials (Mg and SiO_2) dissolve in a uniform fashion without delamination. Each component completely dissolves within hours (Mg) or days/weeks (SiO_2), which is consistent with separate studies of these materials.[8,19]

The findings reported here establish avenues for transient electronic systems that have low modulus, elastic responses to large strain deformation. These characteristics are particularly important in applications that involve integration with biological tissues. Experimental and theoretical results provide insights into the observed behaviors and also suggest routes to further improvements in properties. Sensors of pH and EP represent starting points for the development of more advanced chemical/biological monitors of relevance to envisioned uses of this technology in biomedicine.

Methods. *Fabrication of CMOS Inverters.* p- and n-channel MOSFETs used boron and phosphorus doped Si NMs prepared from n-type silicon on insulator (SOI, top silicon ~260 nm, SOITEC, France) wafers. Lightly doped boron regions for the p-wells (p^-) were defined at 550 °C using spin-on dopant (SOD, Filmtronics, U.S.A.). Heavily doped p^+ and n^+ regions for source and drain electrodes of each p-MOSFET and n-MOSFET were formed at 1050 and 950 °C, respectively. Removal of the underlying box oxide (SiO_2) by wet etching with HF released the device silicon layer from the SOI wafer and allowed transfer printing onto a spin-cast bilayer of PMMA/D-PI on a silicon substrate. Doped Si NMs were isolated by RIE (Plasmatherm) with sulfur hexafluoride (SF_6). PECVD of SiO_2 (~50 nm) formed the gate dielectric. Contact openings for source and drain electrodes were defined by using a buffered oxide etchant (BOE, Transene Company, U.S.A.). A layer of electron beam evaporated Mg (300 nm) served as the source, drain, and gate electrodes, as well as the interconnects. Another thin layer of PECVD SiO_2 encapsulated the devices, except for source, drain, and gate contact pads. A layer of D-PI cast on top of the structure completed the stack. Dry etching completely through the polymer and oxide films defined the mesh structure. Immersion in acetone washed away the PMMA to release the entire system from the silicon substrate, thereby allowing its retrieval onto the surface of a PDMS. After eliminating the base exposed layer of D-PI by oxygen RIE, transfer printing delivered the system onto a biodegradable elastomer (POC). Removing the top layer of D-PI by oxygen RIE completed the process.

Fabrication of pH Sensors. The fabrication began with doping of the Si NMs (p-type, 300 nm) with phosphorus or boron at 950~1050 °C on SOI wafers. The Si NMs were patterned into Si NRs (width, 40 μm; length, 500 μm) by RIE with SF_6 gas. A thin layer of Mg (300 nm thick) deposited by electron beam evaporation (E-beam) served as the source, drain electrodes, and interconnectors. A layer of SiO_2 (300 nm thick) formed by PECVD formed the interlayer dielectrics with sensing windows and contact pads defined by BOE. All other fabrication procedures were similar to those described for the CMOS inverters.

Fabrication of Electrophysiological (EP) Sensors. The fabrication began with casting PMMA/D-PI layers onto a glass slide. Photolithographic patterning of a layer of Mg (300 nm) defined the layout of the EP sensors. A thin layer of SiO_2 (100 nm) formed by PECVD served as the interlayer dielectric with contact pads opened by etching with BOE to allow bonding to an anisotropic conductive film (ACF) cable. All other fabrication procedures were similar to those described for the CMOS inverters.

Electrical Characterization of pH Sensors. The Si NRs were cleaned by exposure to ultraviolet induced ozone for 3 min. Coating with APTES (Sigma-Aldrich, U.S.A.) occurred by immersion in a 1% ethanol solution of APTES for 20 min, rinsing with ethanol three times, and then heating at 80 °C for 10 min. ACF cables connected to bonding pads enabled external data acquisition. Measurements were performed during partial immersion in PBS with various pH values between 3 and 10. A Ag/AgCl reference electrode was placed in the center of the solutions and a floating gate voltage defined the quiescent conductance of the Si NRs. After a short period of stabilization, a semiconductor analyzer (4155C, Agilent, U.S.A.) recorded the conductance of the Si NRs for several seconds in the solutions with various pH from 3 to 10.

Electrical Measurements of Electrophysiological (EP) Sensors. A capacitive EP sensor was connected with ACF cable to a preamplifier with ultrahigh input impedance and extremely low-input capacitance (OPA124, Texas Instruments, U.S.A.; impedance = 10^{14} Ω, 3 pF). This system provided a near-unity gain at the preamplifier, allowing EP signal measurement through an insulation layer (SiO_2). Details of the circuit appear elsewhere.[32] The amplifier and filter units enabled tunable gain (60−80 dB) for ECGs and EMGs. The passband of the circuit was digitally varied using LabVIEW software (National Instruments, U.S.A.). The system was set to a gain of 60 dB in the range of 0.5−100 Hz for ECG; a gain of 80 dB in the range of 10−500 Hz for EMG. The acquired signals were sampled at 1 kHz by an analog-to-digital convertor (NI USB-6363, National Instruments, U.S.A.) and displayed on a computer screen.

Dissolution Tests for Doped Si NRs. The test structures for studying dissolution behaviors of doped Si NRs were formed on a SOI wafer (top Si: ~200 nm, SOITEC, France) by photolithography and RIE. Insoluble materials, such as gold (~150 nm thick) and PI (~1 μm thick) served as source/drain electrodes and encapsulation layers, respectively. The samples were immersed into ~50 mL of phosphate buffer solutions (PBS, 0.1 M, pH 4−10, Sigma-Aldrich, U.S.A.) at a temperature of 37 °C. The samples were removed from the solution at regular time intervals to measure the conductance with a semiconductor analyzer (4155C, Agilent, U.S.A.). The solution was replaced every other day.

■ ASSOCIATED CONTENT

Ⓢ Supporting Information

Supplementary Figures 1−6 and movies 1−3 provide additional information for the results described throughout the main text. This material is available free of charge via the Internet at http://pubs.acs.org.

■ AUTHOR INFORMATION

Corresponding Author

*E-mail: jrogers@illinois.edu.

DOI: 10.1021/nl503997m
Nano Lett. 2015, 15, 2801−2808

Author Contributions

The manuscript was written through contributions of all authors. All authors have given approval to the final version of the manuscript.

S.-W.H., C.H.L., and H.C. contributed equally.

Notes

The authors declare no competing financial interest.

■ ACKNOWLEDGMENTS

H.C. is a Howard Hughes Medical Institute International Student Research fellow. Support for the research was provided by an NSF INSPIRE grant.

■ REFERENCES

(1) Patolsky, F.; Lieber, C. M. *Mater. Today* **2005**, *8*, 20−28.
(2) Tian, B.; Zheng, X.; Kempa, T. J.; Fang, Y.; Yu, N.; Yu, G.; Huang, J.; Lieber, C. M. *Nature* **2007**, *449*, 885−890.
(3) Gao, X. P. A.; Zheng, G.; Lieber, C. M. *Nano Lett.* **2010**, *10*, 547−552.
(4) Bettinger, C. J.; Bao, Z. *Adv. Mater.* **2010**, *22*, 651−655.
(5) Irimia-Vladu, M.; Troshin, P. A.; Reisinger, M.; Shmygleva, L.; Kanbur, Y.; Schwabegger, G.; Bodea, M.; Schwödiauer, R.; Mumyatov, A.; Fergus, J. W.; Razumov, V. F.; Sitter, H.; Sariciftci, N. S.; Bauer, S. *Adv. Funct. Mater.* **2010**, *20*, 4069−4076.
(6) Irimia-Vladu, M.; Glowacki, E. D.; Troshin, P. A.; Schwabegger, G.; Leonat, L.; Susarova, D. K.; Krystal, O.; Ullah, M.; Kanbur, Y.; Bodea, M. A.; Razumov, V. F.; Sitter, H.; Bauer, S.; Sariciftci, N. S. *Adv. Mater.* **2012**, *24*, 375−380.
(7) Tao, H.; Brenckle, M. A.; Yang, M.; Zhang, J.; Liu, M.; Siebert, S. M.; Averitt, R. D.; Mannoor, M. S.; McAlpine, M. C.; Rogers, J. A.; Kaplan, D. L.; Omenetto, F. G. *Adv. Mater.* **2012**, *24*, 1067−1072.
(8) Hwang, S.-W.; Tao, H.; Kim, D.-H.; Cheng, H.; Song, J.-K.; Rill, E.; Brenckle, M. A.; Panilaitis, B.; Won, S. M.; Kim, Y. S.; Song, Y. M.; Yu, K. J.; Ameen, A.; Li, R.; Su, Y.; Yang, M.; Kaplan, D. L.; Zakin, M. R.; Slepian, M. J.; Huang, Y.; Omenetto, F. G.; Rogers, J. A. *Science* **2012**, *337*, 1640−1644.
(9) Hwang, S.-W.; Huang, X.; Seo, J.-H.; Song, J.-K.; Kim, S.; Hage-Ali, S.; Chung, H.-J.; Tao, H.; Omenetto, F. G.; Ma, Z.; Rogers, J. A. *Adv. Mater.* **2013**, *25*, 3526−3531.
(10) Hwang, S.-W.; Kim, D.-H.; Tao, H.; Kim, T.-I.; Kim, S.; Yu, K. J.; Panilaitis, B.; Jeong, J.-W.; Song, J.-K.; Omenetto, F. G.; Rogers, J. A. *Adv. Funct. Mater.* **2013**, *23*, 4087−4093.
(11) Dagdeviren, C.; Hwang, S.-W.; Su, Y.; Kim, S.; Cheng, H.; Gur, O.; Haney, R.; Omenetto, F. G.; Huang, Y.; Rogers, J. A. *Small* **2013**, *9*, 3398−3404.
(12) Kim, Y. J.; Chun, S.-E.; Whitacre, J.; Bettinger, C. J. *J. Mater. Chem. B* **2013**, *1*, 3781.
(13) Kim, Y. J.; Wu, W.; Chun, S.-E.; Whitacre, J. F.; Bettinger, C. J. *Proc. Natl. Acad. Sci. U.S.A.* **2013**, *110*, 20912−20917.
(14) Hwang, S.-W.; Park, G.; Cheng, H.; Song, J.-K.; Yin, L.; Kim, J.-H.; Omenetto, F. G.; Huang, Y.; Lee, K.-M.; Rogers, J. A. *Adv. Mater.* **2014**, *26*, 1992−2000.
(15) Hwang, S.-W.; Song, J.-K.; Huang, X.; Cheng, H.; Kang, S.-K.; Kim, B. H.; Kim, J.-H.; Yu, S.; Huang, Y.; Rogers, J. A. *Adv. Mater.* **2014**, *26*, 3905−3911.
(16) Hwang, S.-W.; Park, G.; Edwards, C.; Corbin, E. A.; Kang, S.-K.; Cheng, H.; Song, J.-K.; Kim, J.-H.; Yu, S.; Ng, J.; Lee, J. E.; Kim, J.; Yee, C.; Bhaduri, B.; Su, Y.; Omennetto, F. G.; Huang, Y.; Bashir, R.; Godard, L.; Popescu, G.; Lee, K.-M.; Rogers, J. A. *ACS Nano* **2014**, *8*, 5843−5851.
(17) Zhou, W.; Dai, X.; Fu, T.-M.; Xie, C.; Liu, J.; Lieber, C. M. *Nano Lett.* **2014**, *14*, 1614−1619.
(18) Yin, L.; Cheng, H.; Mao, S.; Haasch, R.; Liu, Y.; Xie, X.; Hwang, S.-W.; Jain, H.; Kang, S.-K.; Su, Y.; Li, R.; Huang, Y.; Rogers, J. A. *Adv. Funct. Mater.* **2014**, *24*, 645−658.
(19) Kang, S.-K.; Hwang, S.-W.; Cheng, H.; Yu, S.; Kim, B. H.; Kim, J.-H.; Huang, Y.; Rogers, J. A. *Adv. Funct. Mater.* **2014**, *24*, 4427−4434.
(20) Kim, D.-H.; Lu, N.; Ma, R.; Kim, Y.-S.; Kim, R.-H.; Wang, S.; Wu, J.; Won, S. M.; Tao, H.; Islam, A.; Yu, K. J.; Kim, T.-I.; Chowdhury, R.; Ying, M.; Xu, L.; Li, M.; Chung, H.-J.; Keum, H.; McCormick, M.; Liu, P.; Zhang, Y.-W.; Omenetto, F. G.; Huang, Y.; Coleman, T.; Rogers, J. A. *Science* **2011**, *333*, 838−843.
(21) Kim, D.-H.; Ghaffari, R.; Lu, N.; Rogers, J. A. *Annu. Rev. Biomed. Eng.* **2012**, *14*, 113−128.
(22) Kim, R.-H.; Bae, M.-H.; Kim, D. G.; Cheng, H.; Kim, B. H.; Kim, D.-H.; Li, M.; Wu, J.; Du, F.; Kim, H.-S.; Kim, S.; Estrada, D.; Hong, S. W.; Huang, Y.; Pop, E.; Rogers, J. A. *Nano Lett.* **2011**, *11*, 3381−3886.
(23) Webb, C. R.; Bonifas, A. P.; Behnaz, A.; Zhang, Y.; Yu, K. J.; Cheng, H.; Shi, M.; Bian, Z.; Liu, Z.; Kim, Y.-S.; Yeo, W.-H.; Park, J. S.; Song, J.; Li, Y.; Huang, Y.; Gorbach, A. M.; Rogers, J. A. *Nat. Mater.* **2013**, *12*, 938−944.
(24) Vezenov, D. V.; Noy, A.; Rozsnyai, L. F.; Lieber, C. M. *J. Am. Chem. Soc.* **1997**, *119*, 2006−2015.
(25) Cui, Y.; Wei, Q. Q.; Park, H. K.; Lieber, C. M. *Science* **2001**, *293*, 1289−1292.
(26) Penner, R. M. *Annu. Rev. Anal. Chem.* **2012**, *5*, 461−485.
(27) Chen, Y.; Wang, X.; Erramilli, S.; Mohantya, P. *Appl. Phys. Lett.* **2006**, *89*, 223512.
(28) Park, I.; Li, Z.; Pisano, A. P.; Williams, R. S. *Nanotechnology* **2010**, *21*, 015501.
(29) Tian, B.; Cohen-Kami, T.; Qing, Q.; Duan, X.; Xie, P.; Lieber, C. M. *Science* **2010**, *329*, 830−834.
(30) Chen, S.; Bomer, J. G.; Carlen, E. T.; Berg, A. V. D. *Nano Lett.* **2011**, *11*, 2334−2341.
(31) Yang, J.; Webb, A. R.; Ameer, G. A. *Adv. Mater.* **2004**, *16*, 511−516.
(32) Jeong, J.-W.; Kim, M. K.; Cheng, H.; Yeo, W.-H.; Huang, X.; Liu, Y.; Zhang, Y.; Huang, Y.; Rogers, J. A. *Adv. Healthcare Mater.* **2014**, *3*, 642−648.

DOI: 10.1021/nl503997m
Nano Lett. 2015, 15, 2801−2808